https://doi.org/10.5194/egusphere-2025-4584
Preprint. Discussion started: 25 September 2025

Transported African Dust in the Lower Marine Atmospheric Boundary Layer is Internally Mixed with Sea Salt Contributing to Increased Hygroscopicity and a Lower Lidar Depolarization Ratio

Sujan Shrestha[1], Robert E. Holz[2*], Willem J. Marais[2], Zachary Buckholtz[2], Ilya Razenkov[2], Edwin Eloranta[2], Jeffrey S. Reid[3], Hope E. Elliott[1], Nurun Nahar Lata[4], Zezhen Cheng[4], Swarup China[4], Edmund Blades[1], Albert D. Ortiz[1], Rebecca Chewitt-Lucas[5], Alyson Allen[1], Devon Blades[1], Ria Agrawal[1], Elizabeth A. Reid[3], Jesus Ruiz-Plancarte[6], Anthony Bucholtz[6], Ryan Yamaguchi[6], Qing Wang[6], Thomas Eck[7], Elena Lind[7], Mira L. Pöhlker[8], Andrew P. Ault[9], Cassandra J. Gaston[1*]

[1]Department of Atmospheric Sciences, Rosenstiel School of Marine, Atmospheric, and Earth Science, University of Miami, FL, USA

[2]Space Science and Engineering Center (SSEC), University of Wisconsin-Madison, WI, USA

[3]U.S. Naval Research Laboratory, Monterey, CA, USA

[4]Environmental Molecular Sciences Laboratory, Pacific Northwest National Laboratory, Richland, WA, USA

[5]Caribbean Institute for Meteorology and Hydrology, Barbados

[6]Department of Meteorology, Naval Postgraduate School, Monterey, CA, USA

[7]NASA Goddard Space Flight Center, Greenbelt, MD, USA

[8]Atmospheric Microphysics Department, Leibniz Institute for Tropospheric Research, Leipzig, Germany

[9]Department of Chemistry, University of Michigan, MI, USA

*Corresponding Author: Cassandra J. Gaston: Email: cgaston@miami.edu, Phone: (305)-421-4979 and Robert E. Holz: Email: reholz@ssec.wisc.edu

https://doi.org/10.5194/egusphere-2025-4584
Preprint. Discussion started: 25 September 2025

Abstract

Saharan dust is transported across the Atlantic, yet the chemical, physical, and morphological transformations dust undergoes within the marine atmospheric boundary layer (MABL) remain poorly understood. These transformations are critical for understanding dust's radiative and geochemical impacts, representation in atmospheric models, and detection via lidar remote sensing. Here, we present coordinated observations from the Office of Naval Research's Moisture and Aerosol Gradients/Physics of Inversion Evolution (MAGPIE) August 2023 campaign at Ragged Point, Barbados. These include vertically resolved single-particle analyses, mass concentrations of dust and sea spray, and High Spectral Resolution Lidar (HSRL) retrievals. Single-particle data show that dust within the Saharan Air Layer (SAL) remains externally mixed, with a corresponding high HSRL-derived linear depolarization ratio (LDR) of ~0.3. However, at lower altitudes, dust becomes internally mixed with sea spray, resulting in increased particle sphericity likely due to an increase in hygroscopicity, which suppresses the LDR signal to below 0.1 even in the presence of high dust loadings (e.g., ~120 $\mu g/m^3$). The low depolarization in the presence of high dust in the MABL is likely due to a combination of the differences between the single scattering properties of dust and spherical particles, and the potential modification of the dust optical properties from an increased hygroscopicity of dust caused by the mixing with sea salt in the humid MABL. These results highlight the importance of the aerosol particle mixing state when interpreting LDR-derived dust retrievals and estimating surface dust concentrations in satellite products and atmospheric models.

https://doi.org/10.5194/egusphere-2025-4584
Preprint. Discussion started: 25 September 2025

1. Introduction

The transport of Saharan dust across the North Tropical Atlantic Basin throughout the year is one of the largest aerosol phenomena observable from space. The most intensive events often occur during the boreal summer when large quantities of dust are lofted and advected westward by trade winds within the Saharan Air Layer (SAL), a well-defined elevated layer extending from ~2 to 5 km above mean sea level (e.g., Carlson and Prospero, 1972; Karyampudi et al., 1999; Adams et al., 2012; Tsamalis et al., 2013; Mehra et al., 2023). This conceptual model of African dust transport is frequently reinforced by satellite and ground-based remote sensing, particularly lidar (Burton et al., 2012, 2015), multi-angle imager (Kalashnikova et al., 2013), polarimetric (Huang et al., 2015) or combination of these observations (Moustaka et al., 2025) that rely on dust's asphericity to differentiate coarse mode dust from other aerosol sources such as hydrated sea spray. These techniques often detect little dust within the lower marine atmospheric boundary layer (MABL). However, it is well known that exceptionally high dust concentrations are often directly measured in the MABL (e.g., Reid et al., 2003b; Zuidema et al., 2019; Elliott et al., 2024; Mayol-Bracero et al., 2025) and these layers are regularly forecast by operational dust transport models (Xian et al., 2019). This contradiction between the common conceptual model fueled by remote sensing of elevated dust layers versus evidence of significant near-surface dust mass concentrations by in situ observations raises a critical question, is there an observational gap in the detection and characterization of dust within the MABL?

Among the methods to speciate airborne dust from other aerosol particle types, the most common benchmark is the use of lidar's linear depolarization ratio (LDR). The LDR is based on a lidar's range-resolved measurement of the fraction of backscattered light by aerosol particles that become depolarized from the original polarized laser pulse. Backscattered light from

https://doi.org/10.5194/egusphere-2025-4584
Preprint. Discussion started: 25 September 2025

homogeneous spherical particles, such as hydrated sea salt, has low depolarization (e.g., LDR remains minimal) whereas particles with asymmetry such as dry, irregular dust will return a partially depolarized signal, typically ~0.25-0.40 (Murayama et al., 1999; Ansmann et al., 2012; Burton et al., 2012; Freudenthaler et al., 2009; Sakai et al., 2010; Groß et al., 2016).

The assertion that dust can be isolated from other aerosol types such as in the references above is well supported by both theoretical foundations and numerous observations of elevated dust plumes. An important assumption in the detection of dust via the LDR is that the dust is not hygroscopic. In situ observations of dust hygroscopicity in the MABL, typically using the standard technique of drying and subsequently rehydrating particles ahead of nephelometer measurements (Orozco et al., 2016), have suggested MABL dust is not significantly hygroscopic (Li-Jones et al., 1998; Zhang et al., 2014). Thus, it is often assumed that dust in the humid MABL will retain its aspherical shape and remain tracible via the LDR. However, even freshly emitted dust or that which is sampled well within a dust plume can contain soluble minerals that should be inherently hygroscopic and could affect detection of dust via the LDR (Koehler et al., 2007; Reid et al., 2003a).

Contradictory observations have introduced uncertainty in the interpretation of lidar observations for dust detection in the MABL. For example, during the SALTRACE campaign in Barbados, lidar-derived LDR measurements within the lower MABL were 0.15 ± 0.02, suggesting approximately equal parts spherical and non-spherical particles, despite in-situ observations indicating surface dust mass concentrations as high as 40 $\mu g/m^3$ (Groß et al., 2016; Weinzierl et al., 2017). Groß et al. (2016) also reported that dust mass concentrations exceeding 40 $\mu g/m^3$ could be underestimated by up to 50% by lidar-derived depolarization measurements, in part due to the dominant influence of sea spray in the MABL that introduces large

https://doi.org/10.5194/egusphere-2025-4584
Preprint. Discussion started: 25 September 2025

concentrations of hydrated, spherical particles that reduce the overall depolarization signal. Tsamalis et al. (2013) emphasized that the polluted dust aerosol type is often misclassified or detected less often in spaceborne CALIOP observations due to low depolarization signals resulting from dust mixing with other aerosol types such as biomass burning, marine or anthropogenic aerosols (Yang et al., 2022; Kong et al., 2022). The relationship between dust mass and depolarization has important implications for how the depolarization ratio is used to infer surface-level dust concentrations in air quality forecasts and climate models. Since satellite retrievals and column-integrated techniques lack vertical resolution, they may fail to capture such near-surface morphological changes in dust (Li et al., 2020). If depolarization-based methods underestimate dust presence near the surface under marine conditions, it could introduce systematic errors in dust-related radiative forcing and deposition estimates. A similar concern exists for multi-angle imagers and polarimetric retrievals that depend on assumptions of particle asymmetry to detect and quantify dust.

During August 2023, the Office of Naval Research (ONR) initiated the Moisture and Aerosol Gradient/Physics of Inversion Evolution (MAGPIE) field campaign at the University of Miami's Barbados Atmospheric Chemistry Observatory (BACO) at Ragged Point, Barbados to map the inhomogeneity of the MABL. Central to MAGPIE are studies to identify information lost when one conceptualizes the MABL as a series of uniform layers (e.g., surface layer, mixed layer, entrainment or detrainment zones, etc.). While MAGPIE's core objectives focus on atmospheric flows and fluxes with an emphasis on active remote sensing, aerosol particles and their optical closure were implicitly a core mission element because light scattering by these particles can be used to track atmospheric motion. MAGPIE collaborated across U.S. federal agencies, academic institutions, and the Caribbean Institute for Meteorology and Hydrology

https://doi.org/10.5194/egusphere-2025-4584
Preprint. Discussion started: 25 September 2025

(CIMH) and included observations from ground-based aerosol particle samplers and instruments at BACO along with local flights from the Naval Postgraduate School (NPS) CIRPAS Twin Otter (CTO) aircraft. Central to the mission was the University of Wisconsin Space Sciences and Engineering Center's (SSEC) High Spectral Resolution Lidar (HSRL; Eloranta et al., 2008). Here, single particle and bulk analyses are used to evaluate how measured dust and sea salt mass concentrations relate to HSRL-derived LDR. In Section 2, we provide a brief overview of measurements, and in Section 3.1 a timeseries analysis of particle and lidar data, demonstrating nonlinearity between dust and sea salt mass ratios to lidar LDR. In Sections 3.2 and 3.3, we provide vertically resolved single particle data from the CTO aircraft and ground-based samples, respectively, to help explain the anomalies. In Section 4, we provide a discussion and study conclusions.

2. Methods and materials

2.1. Sampling Site and Campaign Overview

Ground-based aerosol particle and lidar measurements were conducted at the BACO site on Ragged Point (13°6′N, 59°37′W) for August 2023. Situated at the easternmost point of the Caribbean, BACO offers an optimal location for intercepting long-range transported Saharan dust with minimal interference from local anthropogenic emissions due to the prevalent Easterly trade winds. Continuous aerosol particle measurements have been conducted there for over 50 years, providing a unique long-term observational record (Prospero et al., 2021; Gaston et al., 2024; Zuidema et al., 2019). The site is equipped with a tower that is 19 m high and is placed atop a 30 m high bluff giving an altitude of ~50 m above sea level.

MAGPIE leveraged multi-platform measurements including aerosol particles collected at the top of the BACO sampling tower and aboard the CTO aircraft to investigate vertical

https://doi.org/10.5194/egusphere-2025-4584
Preprint. Discussion started: 25 September 2025

gradients in aerosol particle chemical and morphological properties. For the 2023 campaign, the focus is centered around the largest dust event of the year observed between August 11-18, 2023. A total of five research flights were conducted during this period, with two samples collected per flight, resulting in ten samples covering a range of altitudes from 30 m to 3 km above mean sea level.

2.2. Surface Sea Salt and Dust Mass Concentrations

Aerosol particles were collected on top of the BACO tower using high-volume samplers with Total Suspended Particulate (TSP) inlets and fitted with cellulose filters (Whatman-41, 20 µm pore size) with particle size cutoff at 80-100 µm in diameter due to the geometry of the rainhat as described in Royer et al. (2023). Procedural filter blanks were collected every five days and processed alongside the daily filter samples. A quarter of each filter was sequentially extracted three times using a total of 20 mL of Milli-Q water to remove soluble components. Following extraction, the filters were combusted at 500 °C overnight in a muffle furnace. The residual ash mass was weighed and corrected for background contributions by subtracting the ash mass obtained from the procedural blank. The net ash mass was multiplied by a correction factor of 1.3 to account for the loss of any soluble or volatile components during the extraction and combustion process (Prospero, 1999; Zuidema et al., 2019). While some soluble components such as halite may be lost during the extraction process, the applied correction factor of 1.3 is intended to conservatively account for these potential losses, supporting more robust dust mass estimates. Moreover, halite is not a major constituent of Saharan dust, as previous studies report its contribution rarely exceeds 3% by weight (Scheuvens et al., 2013), making any bias from its loss during the extraction process unlikely to be significant.

https://doi.org/10.5194/egusphere-2025-4584
Preprint. Discussion started: 25 September 2025

The filtrate collected after dust extraction on the daily filter samples and procedural blanks was then analyzed using ion chromatography (IC) (Dionex Integrion HPIC System; Thermo Scientific). The samples were analyzed in triplicate for cations and anions and corrected for procedural blanks. Details of our IC analysis procedure can be found in Royer et al. (2025). Sodium (Na^+) is commonly used as a conservative tracer for sea spray particles, therefore, the Na^+ concentrations measured by IC analysis were converted to equivalent sea salt concentrations by applying a multiplication factor of 3.252 (Eqn. 1) (Gaston et al, 2024; Prospero, 1979).

$$\text{Sea salt concentration} = [Na^+] * 3.252 \qquad \text{Eqn. 1}$$

2.3. In-situ ground-based aerosol optical measurement

BACO is part of NASA's AErosol RObotic NETwork (AERONET). We used AERONET level 2 aerosol optical depth (AOD at 500 nm) and fine mode AOD (at 500 nm) from the AERONET spectral deconvolution retrieval (O'Neill et al., 2003) to identify the times of dust intrusion during the sampling campaign (Giles et al., 2019; Holben et al., 1998).

2.4. Single-Particle Analysis and Mixing State

Aerosol particle mixing state describes how chemical species are distributed across the particle population (Winkler, 1973; Riemer et al., 2019). Single-particle analysis offers a powerful approach for analyzing this complexity, providing direct insight into the internal composition and variability of individual particles (Ault et al., 2014, 2012; Reid et al., 2003a; Royer et al., 2023). We used computer-controlled scanning electron microscopy (SEM, Quanta from Thermo Fisher Scientific, equipped with a FEI Quanta digital field emission gun at 20 kV and 480 pA electron current) coupled with energy-dispersive X-ray spectroscopy (EDX, Oxford UltimMax100) (CCSEM/EDX) at the Environmental Molecular Sciences Laboratory (EMSL)

https://doi.org/10.5194/egusphere-2025-4584
Preprint. Discussion started: 25 September 2025

located at the Pacific Northwest National Laboratory (PNNL) to characterize single particles. SEM imaging provides both particle sizing and analysis of particle sphericity by measuring the aspect ratio (i.e., ratio of the major axis to minor axis from the 2D projection of particles). EDX spectra are collected for semi-quantitative analysis of the particle elemental composition, and our analysis focused on 16 elements commonly found in atmospheric aerosol particles: carbon (C), nitrogen (N), oxygen (O), sodium (Na), magnesium (Mg), aluminum (Al), silicon (Si), phosphorous (P), sulfur (S), chlorine (Cl), potassium (K), calcium (Ca), vanadium (V), manganese (Mn), iron (Fe), and nickel (Ni). This analysis was conducted for particles collected on the BACO tower and aboard the CTO aircraft.

Ground-based particulate samples for single particle analysis: Ambient aerosol particles were sampled on top of BACO's 19 m tower using a three-stage cascade impactor (Microanalysis Particle Sampler, MPS-3; California Measurements, Inc.), that separates particles into aerodynamic diameter ranges of 2.5-5.0 µm (stage 1), 0.7-2.5 µm (stage 2), and 0.05-0.7 µm (stage 3). Samples were collected for 30 minutes at 2 L/min each day. Particles were deposited onto carbon-coated copper grids (Ted Pella, Inc.) and analyzed using CCSEM/EDX. No conductive coating (e.g., gold or carbon) was applied to the samples collected on the ground as the conductivity of the copper grid bars minimized possible impacts from charging effects. However, Cu signals from CCSEM/EDX were excluded due to interference from the substrate. Elemental signals were considered valid for further analysis only when exceeding a 2% threshold composition detected by EDX spectra. Over 1,000 individual particles were analyzed per sample. Post-processing of CCSEM/EDX data was conducted using a k-means clustering algorithm (Ault et al., 2012; Shen et al., 2016; Royer et al., 2023) to group particles by similarity in composition

https://doi.org/10.5194/egusphere-2025-4584
Preprint. Discussion started: 25 September 2025

and morphology. Clusters were classified into particle types based on their EDX spectra, size, and morphology.

Airborne particulate samples for single particle analysis: Aerosol samples were also collected onboard the CTO using an isokinetic inlet and deposited onto isopore membrane filters (47 mm filter, 0.8 µm pore size). An overview of the airborne sampling technique can be found in the Supporting Information (SI Text S1). The CTO's primary inlet has an intrinsic cutpoint of ~3.5 µm in aerodynamic diameter. Due to limitations associated with Teflon filter material, automated computer-controlled SEM was not feasible, and these airborne samples were analyzed manually using SEM/EDX. To prevent particle charging during imaging, filters were sputtered with a gold-coating of 10 nm thickness prior to analysis. A total of 40, 21, and 52 particles from 250 nm to 25 µm diameter were manually analyzed from samples collected within the SAL, above, and below cloud base heights (CBH), respectively, providing a primarily qualitative assessment. The CBH was identified for each flight as the first maximum in profile relative humidity, typically near saturation. Whenever possible, ground-based measurements were coordinated to coincide with periods when the CTO aircraft intercepted the BACO location or its vicinity. Single particle analysis from aircraft sampling, presented in Figure 3c, serves as a comparative reference to the more comprehensive in-situ ground-based dataset, which includes ~24,000 analyzed particles.

2.5. High Spectral Resolution Lidar (HSRL)

The SSEC HSRL was deployed during the summer 2023 MAGPIE campaign to characterize the vertical distribution of aerosol particle scattering properties over Ragged Point. The HSRL system used in this study can provide range-resolved profiles of particulate backscatter and depolarization at high spatial and temporal resolution. Details on the SSEC

https://doi.org/10.5194/egusphere-2025-4584
Preprint. Discussion started: 25 September 2025

HSRL can be found elsewhere (Razenkov, 2010; Eloranta et al., 2008). Briefly, the SSEC HSRL operates at a wavelength of 532 nm and separates molecular and particulate backscatter signals using a narrowband iodine absorption filter. This configuration enables accurate, independent retrievals of particulate backscatter within close proximity to the ocean surface. At distances beyond 3 km, the extinction-to-backscatter ratio (i.e., the lidar ratio) can be derived as well as extinction. The HSRL also contains an elastic backscatter channel of 1064 nm.

For MAGPIE, the SSEC-HSRL was configured to operate in periods of vertical stare, horizontal stare, and vertical scanning from -0.05° to 18°. For the purposes of this paper, we only utilize vertical data. Extraction of light extinction and the lidar ratio within the MABL are performed using the HSRL in one of its side or vertically scanning modes. While a manuscript is under preparation (Fu et al., 2025, in prep.), for the purpose of this paper we can report from its authors that lidar ratios in the MABL's mixed layer ranged from 20 to 25 sr, and in the SAL was on the order of 40sr. Lidar ratios of 20 sr are consistent with ambient sea salt and 40 sr above the MABL with "dry" dust.

3. Results and discussion

3.1. Temporal variability in surface-level aerosol particle chemistry, AOD and lidar depolarization ratios (LDR) during a major dust event

Figure 1 presents a time series of key aerosol properties observed during the August 2023 MAGPIE intensive operations period, including surface-level dust and sea salt mass concentrations, aerosol optical depth (AOD), and HSRL-derived linear depolarization ratio (LDR) and particulate backscatter. Over the month, median dust and sea salt concentrations were 6 ± 32 and 17 ± 9 µg/m^3, respectively; the median columnar AOD was 0.15 ± 0.19; and the median LDR at 105 m above mean sea level was 0.03 ± 0.03 Notably, a distinct deviation from

https://doi.org/10.5194/egusphere-2025-4584
Preprint. Discussion started: 25 September 2025

these baseline values was observed during a period of Saharan dust intrusion occurring between August 11 and 18, 2023. The dust event led to pronounced changes in the chemical composition and physical properties of aerosol particles observed in Barbados, yet the LDR showed little increase. During this period, the dust mass concentration peaked at 120 µg/m^3 on August 15, comparable to the concentration measured during the major "Godzilla" dust event of 2020 (Elliott et al., 2024; Mayol-Bracero et al., 2025), while inferred sea salt concentrations based on sodium were 27 µg/m^3. The average dust-to-sea salt mass ratio was ~3.4 on dusty days and peaking at 4.8, compared to ~0.40 on non-dusty days, indicating a clear dominance of dust in the lower MABL during the dust intrusion event. Total column AOD (550 nm) closely tracked the trend in surface dust mass concentration and peaked at ~0.75 on August 15, whereas fine mode AOD remained substantially lower (0.12 ± 0.01) (Fig. 1b) indicating that the total AOD was predominantly influenced by coarse-mode particles during the dust period. Notably, this event produced one of the highest AOD recorded in Barbados during the month of August over the past decade (Fig. S1). Additionally, the Extinction Ångstrom Exponent (440-870 nm) from AERONET averaged 0.05 on August 15, compared to 0.30 ± 0.20 for the entire month of August, confirming that the total column aerosol particle loading was dominated by coarse mode particles (Russell et al., 2010).

https://doi.org/10.5194/egusphere-2025-4584
Preprint. Discussion started: 25 September 2025

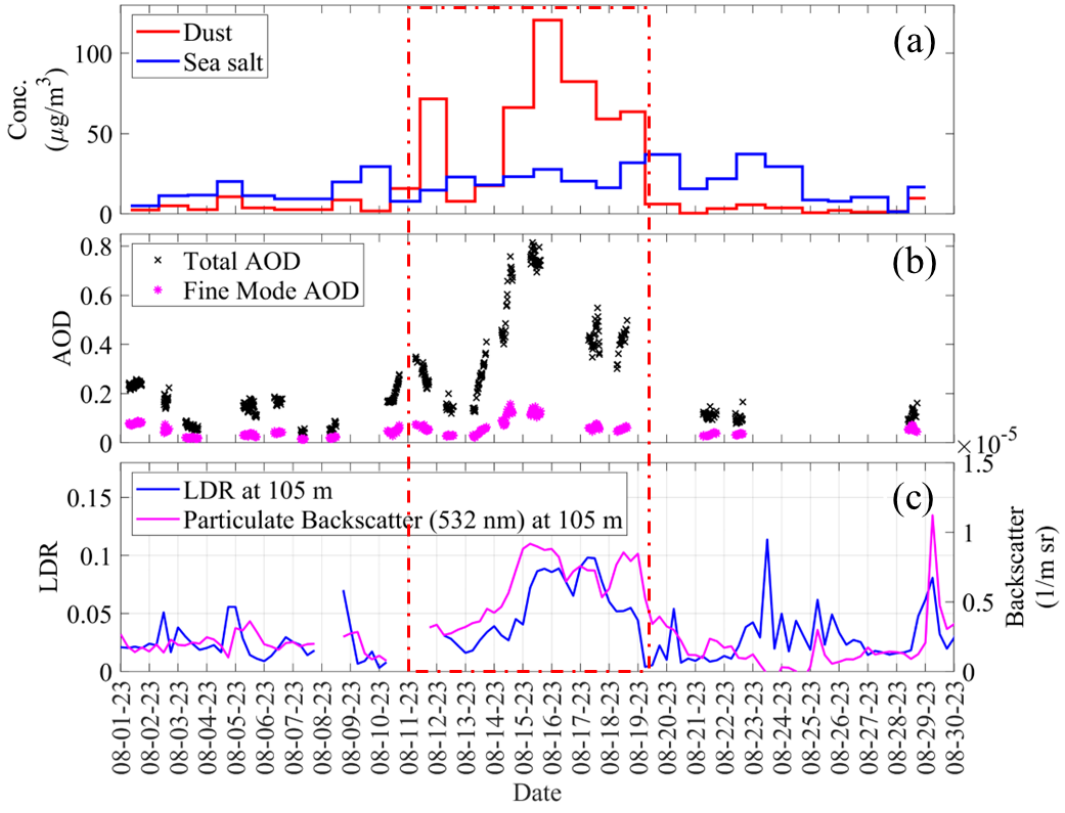

Figure 1. Time series plots for (a) dust and sea salt mass concentrations measured from the top of the BACO tower, (b) AERONET total column and fine mode fraction AODs (at 500 nm) and (c) HSRL- linear depolarization ratio (LDR) and particulate backscatter at 532 nm, averaged over six hours, during the MAGPIE 2023 campaign. The red dashed box represents the major dust event observed during the campaign.

Figure 2a shows the time series of linear depolarization measurements from August 11-18 where a dust layer (as indicated by an LDR of 0.30) is observed aloft (~2-6 km above mean sea level) above Ragged Point. This altitude range is consistent with previous studies that have reported the SAL to typically extend from approximately 1.5 to 5.5 km above mean sea level (Carlson and Prospero, 1972; Groß et al., 2015; Karyampudi and Carlson, 1988; Reid et al.,

https://doi.org/10.5194/egusphere-2025-4584
Preprint. Discussion started: 25 September 2025

2003; Weinzierl et al., 2017). Figure 2a also reveals the temporal variability of LDR during this period and the presence of multiple distinct atmospheric layers. Figure 1c presents the time series of the LDR at 105 m above mean sea level, representing conditions near the surface within the lower MABL for comparison with other ground-based measurements. Although an increase in LDR was observed in the lower MABL during the period of pronounced dust loading, the enhancement was surprisingly small, with values less than 0.10 (Fig. 1c). The finding can be partially explained through scattering physics (e.g., the lidar equation) governing the lidar signals (Hayman and Spuler, 2017). The HSRL particulate depolarization measurement responds to the 180-degree backscatter efficiency of the particulates (lidar ratio). For MAGPIE, the HSRL lidar ratio measurement of dust was ~40 with the MABL having a lidar ratio of ~20, a factor of two different with the marine sourced particles being twice as efficient per scattering cross-section compared to dust at backscattering energy. For an atmosphere with equally weighted extinction between dust and marine aerosol, the measured depolarization will be weighted lower due to the backscatter efficiency difference between the aerosol (i.e., lidar ratio). Figure 2b shows the representative vertical distribution of RH during the dusty period of the study, revealing a distinctly moist MABL characterized by RH values exceeding 80%. Such elevated humidity levels are conducive to the hygroscopic growth of aerosol particles, which can induce morphological and optical changes (Guo et al., 2019; Ji et al., 2025; Titos et al., 2016) that can impact their LDR.

https://doi.org/10.5194/egusphere-2025-4584
Preprint. Discussion started: 25 September 2025

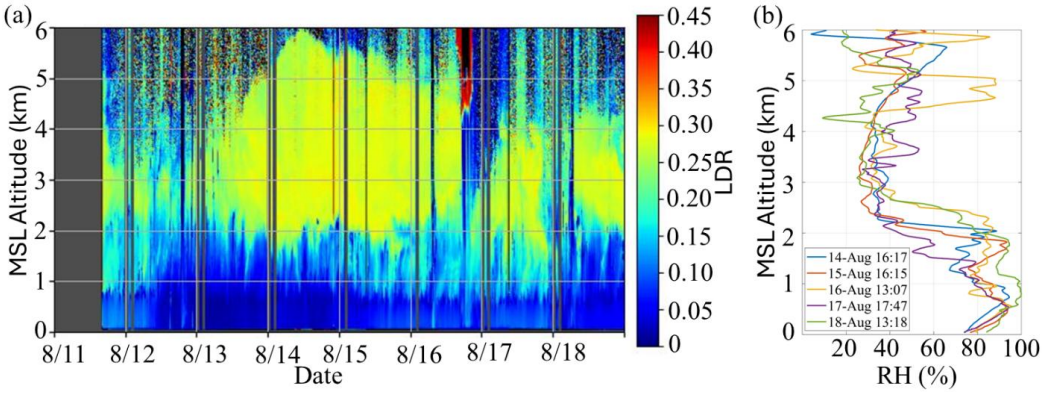

Figure 2. (a) HSRL scan for linear depolarization ratio within 6 km above msl for August 11 -18, 2023. (b) Vertical profiles of relative humidity (RH, %) up to 6 km above mean sea level (MSL) from radiosonde launches at Ragged Point on representative days between August 14 and 18, 2023.

3.2 Vertical Gradients in the LDR and aerosol mixing state

To get a better insight into the influence of a major dust on the vertical structure of the LDR, Figures 3a and b show HSRL data from August 15 (15:00 UTC), the day when Barbados experienced the highest ground-level dust concentration (~120 µg/m³). Figure 3a shows the vertical distribution of particulate backscatter, revealing roughly two aerosol layers: one extending from the lower MABL up to ~2.5 km, and a second from ~2.5 to 5 km. The elevated backscatter in the lower layer is attributed to a higher abundance of a mix of sea spray and dust particles, which are more effective at scattering light under humid marine conditions that were shown in the sounding in Figure 2b to be prevalent in the lower MABL (Fig. 2b). In contrast, the upper layer exhibits reduced particulate backscatter, due to the predominance of larger but less backscattering mineral dust particles. While the backscatter profile shows the relative abundance and scattering characteristics of atmospheric layers, the distinct separation between aerosol

https://doi.org/10.5194/egusphere-2025-4584
Preprint. Discussion started: 25 September 2025

layers is more clearly resolved in the LDR profile shown in Figure 3b. In Fig. 3b, a prominent SAL was observed extending from approximately 1.8 km to 5 km above mean sea level, consistent with the typical SAL altitude range reported in previous studies during summer (Carlson and Prospero, 1972; Groß et al., 2015; Karyampudi and Carlson, 1988; Reid et al., 2003; Tsamalis et al., 2013; Weinzierl et al., 2017). The LDR values within this layer were around 0.30, indicative of a highly depolarizing aerosol regime with mineral dust dominance. This observation is consistent with previous findings that long-range-transported Saharan mineral dust aerosol layers maintain high depolarization values due to their irregular shape (Freudenthaler et al., 2009; Groß et al., 2015). Below the SAL, between 0.7 km and 1.8 km, LDR values were much smaller and ranged from 0.10 to 0.20, typical for aerosol regimes within the humid MABL where mineral dust particles are mixed with spherical particles like sea spray particles (Gasteiger et al., 2017; Tesche et al., 2011). At altitudes below 0.7 km, LDR values were consistently <0.10, commonly taken as being indicative of the dominance of sea spray particles with reduced dust influence. Given that dust concentrations were approximately four times greater than those of sea salt during the peak of the event, we applied a multiple regression approach to estimate the LDR, using Eqn. 2, during the dust event that incorporated measured lidar ratio and dust and sea salt concentrations.

$$LDRexpected = \frac{v_{\perp}^{(d)}}{v_{\parallel}^{(d)} + v_{\parallel}^{(m)}} + \frac{v_{\perp}^{(m)}}{v_{\parallel}^{(d)} + v_{\parallel}^{(m)}} \qquad Eqn.\,2$$

where, $v_{\parallel}^{(d)}$ and $v_{\parallel}^{(m)}$ represent the parallel components, and $v_{\perp}^{(d)}$ and $v_{\perp}^{(m)}$ represent the perpendicular components of the particulate backscatter from dust (“d”) and marine aerosol (“m”) particles, respectively.

https://doi.org/10.5194/egusphere-2025-4584
Preprint. Discussion started: 25 September 2025

This analysis yielded an estimated LDR of 0.17 ± 0.03 during the dust peak, ~2 times higher than the values observed in the lower MABL. The uncertainty associated with our estimated LDR prediction may be larger than the standard deviation reported, as we did not explicitly account for the full-size distribution of sea salt and dust aerosols. In particular, large particles beyond the upper cutpoint (>80 -100 μm) of our bulk dust sampler were not captured. These coarse particles, which are more efficient at depolarizing incident light due to their irregular shape and size, could contribute significantly to the lidar signal. Their absence from the analysis may lead to an underestimation of the true depolarization potential, especially during intense dust events. Details about this estimate calculation and approximations used to derive this estimate are in SI Text S3. This is further illustrated in Fig. 4, which shows the relationship between the dust-to-sea salt mass concentration ratio versus the measured HSRL-derived LDR and estimated LDR from the multiple regression approach. The discrepancy between expected and observed LDR highlights the need to investigate the role of particle composition and mixing state in modulating depolarization signals.

https://doi.org/10.5194/egusphere-2025-4584
Preprint. Discussion started: 25 September 2025

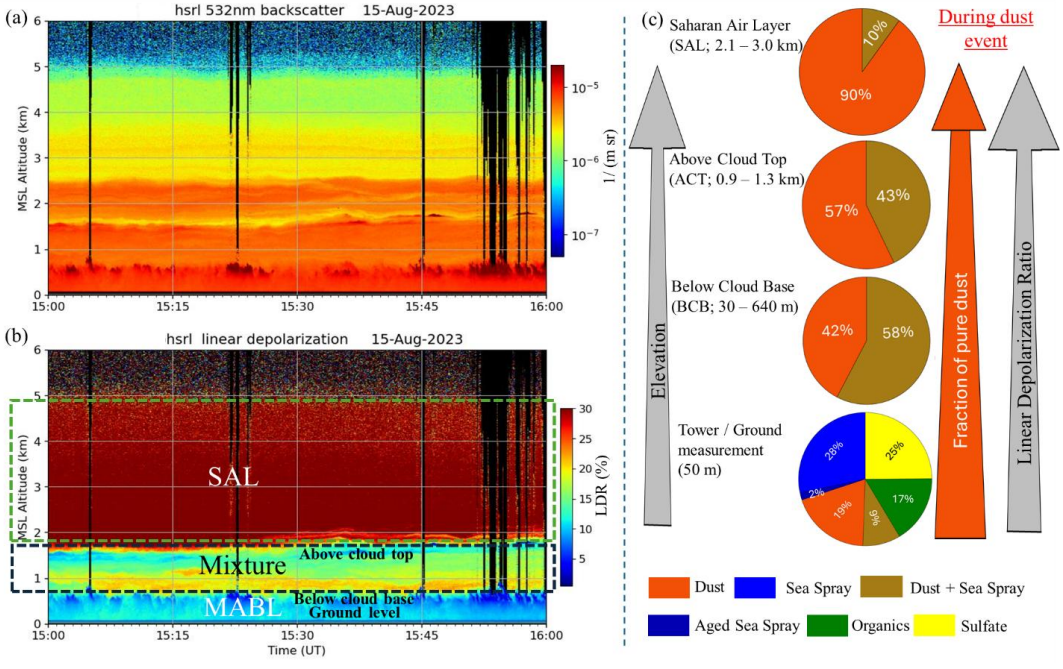

Figure 3. HSRL scan for (a) particulate backscatter at 532 nm and (b) linear depolarization ratio within 6 km above msl for August 15, 2023 (15:00 hrs UTC). (c) Pie chart showing the percentage of the number concentration of detected particle types from single particle analysis at different altitudes: SAL, above cloud base, below cloud top, and ground-based samples collected atop the BACO tower during the dust event. The altitude range where samples collected for single particle analysis were taken are indicated in parentheses next to each corresponding pie chart. Pie charts show that with increased elevation, the fraction of externally mixed dust increased and the linear depolarization ratio (LDR) from the HSRL measurement increased during the dust event.

https://doi.org/10.5194/egusphere-2025-4584
Preprint. Discussion started: 25 September 2025

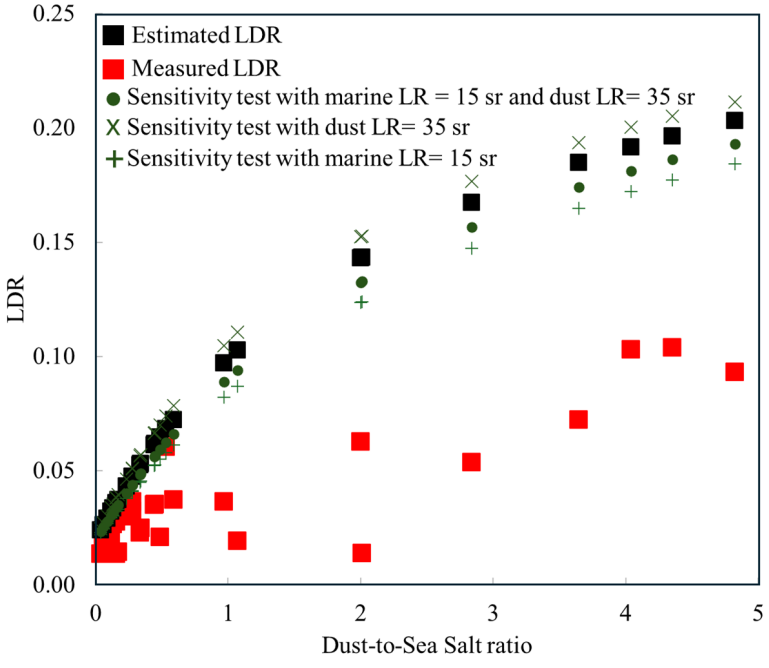

Figure 4. Relationship between the dust-to-sea salt concentration ratio and HSRL-derived LDR at 105 m above ground level during the MAGPIE campaign. Red squares indicate measured LDR values for the full campaign, while black squares represent LDR values estimated from mass concentrations and lidar ratio weighting during the peak dust event. The observed LDR during peak dust event is underestimated by approximately a factor of two. A sensitivity test was conducted using more conservative lidar ratio values for dust and marine aerosols (shown as green plus, cross and circle symbols), and in all such cases the estimated LDR values remained consistently higher than the measured values.

A vertical gradient in aerosol particle mixing state was observed during the Saharan dust intrusion, wherein dust is internally mixed with sea spray at the surface and externally mixed aloft. Single-particle chemical composition and morphology analysis revealed a diverse set of particle types with distinct chemistries and morphologies, including mineral dust, sea spray, aged

https://doi.org/10.5194/egusphere-2025-4584
Preprint. Discussion started: 25 September 2025

sea spray, internally mixed mineral dust and sea spray, sulfates, and organics (Royer et al., 2023; Ault et al., 2012, 2014). Detailed chemical composition of the particle types is presented in SI Text S2 and representative SEM images and corresponding EDX spectra for each particle class are shown in Fig. 5a.

Figure 3c presents the vertical profile of the number fractions of aerosol particle types, averaged over the samples taken during dusty days. From the figure, we can infer that the SAL was predominantly composed of mineral dust particles (90% of the analyzed particles) transported from Northern Africa. The LDR observed within the SAL (0.30) is attributable to the large fraction of mineral dust present in this layer. Additionally, an indifferentiable transition layer between the SAL and the MABL (labeled as “Mixture” in Fig. 3b) exists in the atmosphere, where both sea salt and mineral dust are concurrently present. In the SAL, a fraction of these sea spray particles was internally mixed with mineral dust (10% of the analyzed particles). A comparison of particle composition across altitudes reveals that samples collected above the cloud top contained a slightly higher proportion of mineral dust (57%) compared to internally mixed dust and sea spray particles (43%). In contrast, below the cloud base, this ratio was reversed, with internally mixed dust and sea spray particles making up 58% of the dust and externally mixed dust 42% of the dust particles suggesting a dynamic, vertical exchange of particles within the MABL, possibly facilitated by both cloud processing mechanisms that enhance coagulation as well as updrafts of sea spray that enhance collisions with dust (Matsuki et al., 2010). The presence of a substantial fraction of internally mixed dust and sea spray particles above and below cloud base is expected, given that sea salt is a dominant contributor to cloud droplets (Crosbie et al., 2022). The number fraction of mineral dust particles increased substantially in the MABL during periods of intense dust intrusion, with a distinct peak observed

https://doi.org/10.5194/egusphere-2025-4584
Preprint. Discussion started: 25 September 2025

on August 15 (Fig. 5b). However, particle composition was more variable at the surface compared to aloft, consistent with the proximity to the ocean increasing the presence of marine aerosol particles including sea salts, organics, and sulfates (Fig. 3c). Overall, these observations suggest that the reduced LDR values in the MABL are likely explained, in part, by internally mixed dust and hydrated sea spray particles in the presence of high humidity, resulting in hydrated, more spherical and hence less depolarizing particles.

3.3 Size and Morphology of Different Particle Types at the Surface Level

Internally mixed dust and sea spray particles at the surface exhibited both larger median diameters and smaller aspect ratios compared to either externally mixed mineral dust particles. This morphological evolution is likely due to enhanced particle hygroscopicity in internally mixed dust and sea salt particles, which would explain, in part, the suppressed LDR during the major dust intrusion event. Figures 5c and S2 present the size-resolved average chemical composition of ground-level aerosol samples collected during the dust event. Because significant particle statistics are available from our surface measurements, Fig. 5 focuses only on aerosol particles collected at BACO to understand changes in the aerosol size and morphology across different particle types. A clear compositional shift is observed between submicron and super-micron particles. In the submicron range (particle diameter < 1 μm), organic and sulfate aerosol particles were dominant, with median diameters of 0.45 μm and 0.36 μm, respectively. In contrast, the super-micron size range was dominated by sea spray, mineral dust, and internally mixed dust and sea spray particles. Externally mixed mineral dust collected through our impactor had a number median diameter of ~1.2 μm, while internally mixed dust and sea spray particles exhibited larger median diameters of ~2.0 μm, likely resulting from coagulation and condensation processes occurring during dust descent into the MABL (Kandler et al., 2018).

https://doi.org/10.5194/egusphere-2025-4584
Preprint. Discussion started: 25 September 2025

Figure 5d shows the aspect ratio, a measure for particle sphericity determined with SEM imaging, of different aerosol types as a function of particle size. An aspect ratio of 1 corresponds to a perfectly spherical or cuboid particle, with deviations indicating increased asphericity. As expected, sea spray and sulfate particles exhibited cubic or near-spherical morphologies (Ault et al., 2013; Shao et al., 2022) with the lowest aspect ratios of 1.2. Mineral dust particles were highly irregular in shape, with a median aspect ratio of 1.6 ± 0.7, consistent with previous observations (Barkley et al., 2021; Huang et al., 2020). Notably, internally mixed dust and sea spray particles had a lower median aspect ratio of 1.4 ± 0.6, particularly in super-micron particles (1.4 ± 0.5) compared to submicron particles (1.7 ±1.0). This suggests that dust mixing with sea spray particles may promote the formation of more uniform coatings around mineral dust cores (Formenti et al., 2011) and likely increase the particle hygroscopicity (Guo et al., 2019) at the high RH observed in the lower MABL (Fig. 2b), thereby reducing particle irregularity, especially in larger particles. Therefore, as mineral dust is entrained into the MABL and mixed with sea spray, the dust particles become larger and more spherical in shape. The consistently low LDR values observed in the lower MABL can likely be attributed, in part, to a combination of increased hygroscopicity, size, and sphericity, all of which contribute to a reduced depolarization ratio.

https://doi.org/10.5194/egusphere-2025-4584
Preprint. Discussion started: 25 September 2025

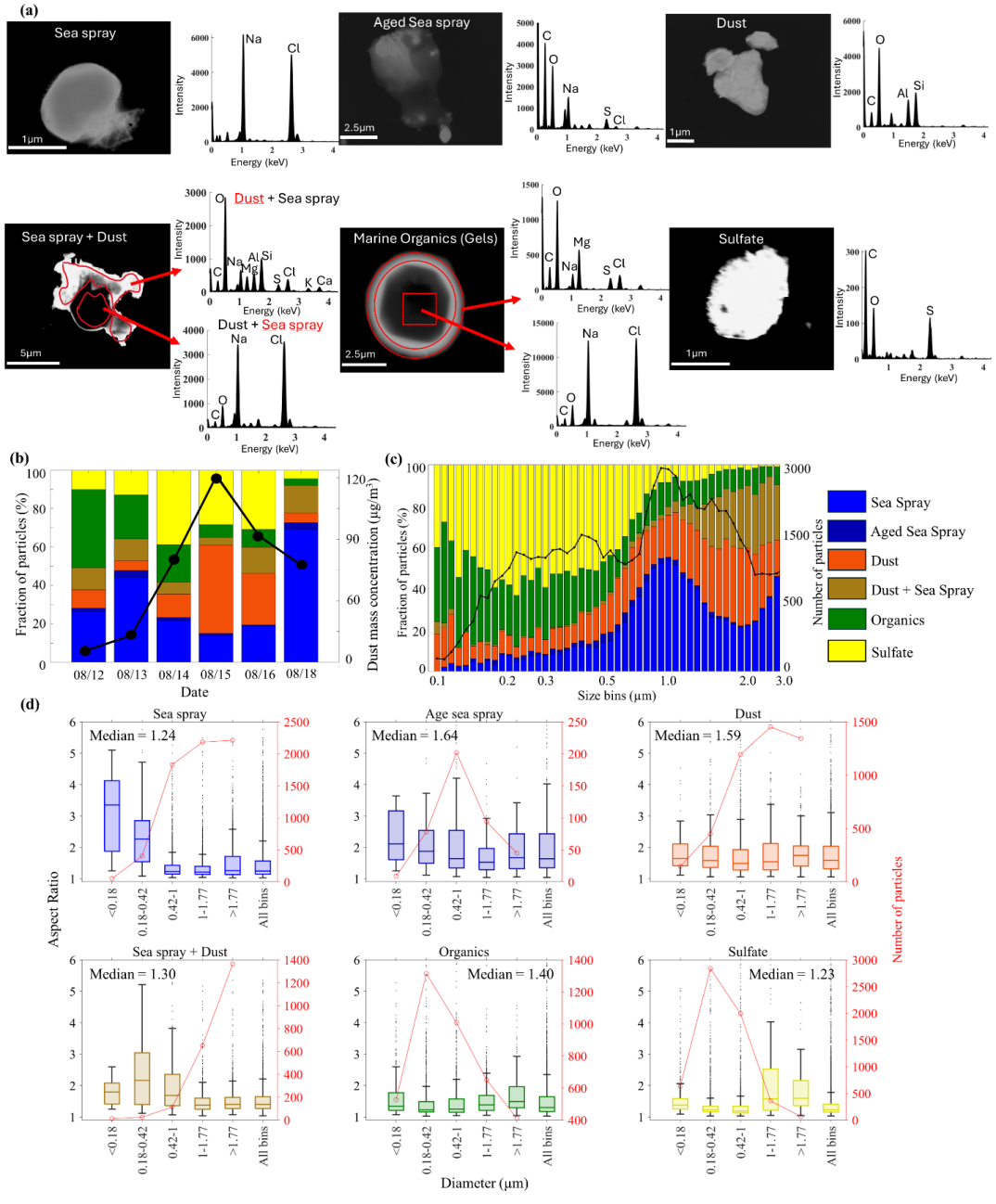

Figure 5. (a) Representative aerosol particle types observed in surface samples by SEM images (left) and EDX spectra (right) in samples collected during the MAGPIE campaign. (b) Temporal

https://doi.org/10.5194/egusphere-2025-4584
Preprint. Discussion started: 25 September 2025

variations in the number fraction of different particle types during the dust event. (c) Number fractions of different particle types plotted as a function of the particle projected area diameter. (d) Box and whisker plot of the aspect ratio of different particle types at different particle size bins. The total number of particles analyzed for each particle type are plotted as a red line. These plots are generated from the single particle CCSEM/EDX analysis of the in-situ samples collected at the top of the 19 m tower at BACO site. Each box-and-whisker plot displays the median (central line), lower and upper quartiles (box edges), minimum and maximum values excluding outliers (whiskers), and any statistical outliers (dots), determined using the 1.5× interquartile range (IQR) method.

4. Conclusions and Atmospheric Implications

Single-particle analysis conducted during the MAGPIE campaign revealed that Saharan dust particles in the MABL are physically and chemically distinct from dust within the SAL aloft. Our results show that in the lower MABL, dust becomes internal mixed with sea spray resulting in an increased size and sphericity, and potentially enhanced hygroscopicity compared to externally mixed dust. These changes, in part, suppress the dust's depolarization (being more spherical) signal and complicate its identification by lidar. Despite peak dust loading (AOD ~0.75; surface dust ~120 µg/m³), HSRL observations showed that LDR values in the lower MABL remained mostly below 0.10, a range typically associated with spherical marine aerosols, even though dust concentrations were ~4.8 times higher than sea salt. This discrepancy is further explained by differences in the scattering efficiency (lidar ratio) of dust and marine aerosols, where dust is about half as efficient at backscattering energy per extinction cross-section (lidar ratio) compared to marine aerosol which weighs the marine aerosol signal in the depolarization measurement by a factor of ~3. These combined effects of morphological transformation and

https://doi.org/10.5194/egusphere-2025-4584
Preprint. Discussion started: 25 September 2025

differential lidar ratios reduce the dust signature in depolarization-based retrievals, complicating its detection and quantification near the surface. The resulting underestimation of surface-level dust by lidar-based depolarization retrievals is of particular concern especially during high-dust events like the one observed during this study, where surface particulate matter (PM) exceeded WHO guidelines for PM_{10} of 45 $\mu g/m^3$ (World Health Organization, 2021) by a factor of nearly three. Moreover, it may help explain similar discrepancies between lidar observations and in situ measurements in other regions where dust is modified through interactions with marine aerosols.

More broadly, these results highlight the importance of integrating vertically resolved lidar data with in-situ single-particle analysis and surface aerosol mass concentrations to improve the interpretation of lidar observations in dust-affected regions. Such integrated approaches are essential because LDR is widely used in satellite retrieval algorithms and atmospheric models to estimate dust volume and mass fractions, calculate dust-related radiative forcing, estimate dust contribution to cloud condensation and ice nucleation profiles, estimate dust deposition to receptor ecosystems, and predict surface air quality (Meloni et al., 2018; Haarig et al., 2017; Müller et al., 2010, 2012; Yang et al., 2012; Marinou et al., 2017; Proestakis et al., 2018; Adebiyi et al., 2023; Mahowald et al., 2005). Without such integrated observations, satellite retrievals and forecasting systems may significantly underestimate dust impacts near the surface, where they matter most for air quality and biogeochemical feedback.

Data Availability

Dust and sea salt mass concentration data and number counts of particle types detected by CCSEM/EDX will be publicly available in the University of Miami data repository.

The HSRL data can be accessed through the University of Wisconsin-Madison SSEC repository at https://hsrl.ssec.wisc.edu/by_site/37/bscat/2025/04/.

https://doi.org/10.5194/egusphere-2025-4584
Preprint. Discussion started: 25 September 2025

The NASA AERONET data can be accessed through https://aeronet.gsfc.nasa.gov.

Author Contribution

Conceptualization of this work was done by SS, RJH, JSR, and CJG. Collection of samples was conducted by SS, WJM, ZB, IR, EE, JSR, EB, ADO, RCL, AA, DB, EAR, JRP, AB, RY, QW, TE, EL, MLP, and CJG, while analysis was done by SS, HEE, NNL, ZC, SC, and RA. The development of method used in this work was done by SS, REH, WJM, EE, JSR, and CJG. Instrumentation used to conduct this work was provided by REH, SC, MLP, and CJG. Formal analysis of data was performed by SS, WJM, and JSR. Validation of data products was performed by SS, RJH, WJM, JSR, AA, and CJG. Data visualization was performed by SS. Supervision and project administration duties were done by RJH, JSR, and CJG. SS wrote the original draft for publication, and all the co-authors reviewed and edited this work.

Competing Interests

The contact author has declared that none of the authors has any competing interests.

Acknowledgements

We thank the family of HC Manning and the Herbert C Manning Trust for providing access to their land at Ragged Point in Barbados. We thank Jeremy Bougoure at EMSL for his help with the Au sputter coating of our filter samples.

Financial Support

CJG and SS acknowledge the Office of Naval Research (ONR) grants N00014-23-1-2861 and N000142512003 and NSF MRI grant 2215875. A portion of this research was performed on project awards (10.46936/lser.proj.2021.51900/60000361 and

https://doi.org/10.5194/egusphere-2025-4584
Preprint. Discussion started: 25 September 2025

https://doi.org/10.46936/ltds.proj.2023.61072/60012372) from the Environmental Molecular Sciences Laboratory, a DOE Office of Science User Facility sponsored by the Biological and Environmental Research program. REH, WJM, ZB, IR and EE were supported under ONR grant N000142412736. JSR and EAR were supported under ONR grant O2507-017-017-112205. AB was supported under ONR grant N0001423WX01787. QW, JRP and RY were supported under ONR grant N0001424WX02429. APA acknowledges support from ONR grant N000142512003 and DOE grant DE-SC0025196.

References

Adams, A. M., Prospero, J. M., and Zhang, C.: CALIPSO-Derived Three-Dimensional Structure of Aerosol over the Atlantic Basin and Adjacent Continents, J. Clim., 25, 6862–6879, https://doi.org/10.1175/JCLI-D-11-00672.1, 2012.

Adebiyi, A., Kok, J. F., Murray, B. J., Ryder, C. L., Stuut, J.-B. W., Kahn, R. A., Knippertz, P., Formenti, P., Mahowald, N. M., Pérez García-Pando, C., Klose, M., Ansmann, A., Samset, B. H., Ito, A., Balkanski, Y., Di Biagio, C., Romanias, M. N., Huang, Y., and Meng, J.: A review of coarse mineral dust in the Earth system, Aeolian Res., 60, 100849, https://doi.org/10.1016/j.aeolia.2022.100849, 2023.

Ault, A. P., Peters, T. M., Sawvel, E. J., Casuccio, G. S., Willis, R. D., Norris, G. A., and Grassian, V. H.: Single-Particle SEM-EDX Analysis of Iron-Containing Coarse Particulate Matter in an Urban Environment: Sources and Distribution of Iron within Cleveland, Ohio, Environ. Sci. Technol., 46, 4331–4339, https://doi.org/10.1021/es204006k, 2012.

Ault, A. P., Moffet, R. C., Baltrusaitis, J., Collins, D. B., Ruppel, M. J., Cuadra-Rodriguez, L. A., Zhao, D., Guasco, T. L., Ebben, C. J., Geiger, F. M., Bertram, T. H., Prather, K. A., and Grassian, V. H.: Size-Dependent Changes in Sea Spray Aerosol Composition and Properties with Different Seawater Conditions, Environ. Sci. Technol., 47, 5603–5612, https://doi.org/10.1021/es400416g, 2013.

Ault, A. P., Guasco, T. L., Baltrusaitis, J., Ryder, O. S., Trueblood, J. V., Collins, D. B., Ruppel, M. J., Cuadra-Rodriguez, L. A., Prather, K. A., and Grassian, V. H.: Heterogeneous Reactivity of Nitric Acid with Nascent Sea Spray Aerosol: Large Differences Observed between and within Individual Particles, J. Phys. Chem. Lett., 5, 2493–2500, https://doi.org/10.1021/jz5008802, 2014.

Barkley, A. E., Olson, N. E., Prospero, J. M., Gatineau, A., Panechou, K., Maynard, N. G., Blackwelder, P., China, S., Ault, A. P., and Gaston, C. J.: Atmospheric Transport of North African Dust-Bearing Supermicron Freshwater Diatoms to South America: Implications for Iron Transport to the Equatorial North Atlantic Ocean, Geophys. Res. Lett., 48, https://doi.org/10.1029/2020GL090476, 2021.

https://doi.org/10.5194/egusphere-2025-4584
Preprint. Discussion started: 25 September 2025

Burton, S. P., Ferrare, R. A., Hostetler, C. A., Hair, J. W., Rogers, R. R., Obland, M. D., Butler, C. F., Cook, A. L., Harper, D. B., and Froyd, K. D.: Aerosol classification using airborne High Spectral Resolution Lidar measurements – methodology and examples, Atmos. Meas. Tech., 5, 73–98, https://doi.org/10.5194/amt-5-73-2012, 2012.

Burton, S. P., Hair, J. W., Kahnert, M., Ferrare, R. A., Hostetler, C. A., Cook, A. L., Harper, D. B., Berkoff, T. A., Seaman, S. T., Collins, J. E., Fenn, M. A., and Rogers, R. R.: Observations of the spectral dependence of linear particle depolarization ratio of aerosols using NASA Langley airborne High Spectral Resolution Lidar, Atmos. Chem. Phys., 15, 13453–13473, https://doi.org/10.5194/acp-15-13453-2015, 2015.

Carlson, T. N. and Prospero, J. M.: The Large-Scale Movement of Saharan Air Outbreaks over the Northern Equatorial Atlantic, J. Appl. Meteorol. Clim., 11, 283–297, https://doi.org/https://doi.org/10.1175/1520-0450(1972)011< 0283:TLSMOS>2.0.CO;2, 1972.

Crosbie, E., Ziemba, L. D., Shook, M. A., Robinson, C. E., Winstead, E. L., Thornhill, K. L., Braun, R. A., MacDonald, A. B., Stahl, C., Sorooshian, A., van den Heever, S. C., DiGangi, J. P., Diskin, G. S., Woods, S., Bañaga, P., Brown, M. D., Gallo, F., Hilario, M. R. A., Jordan, C. E., Leung, G. R., Moore, R. H., Sanchez, K. J., Shingler, T. J., and Wiggins, E. B.: Measurement report: Closure analysis of aerosol–cloud composition in tropical maritime warm convection, Atmos. Chem. Phys., 22, 13269–13302, https://doi.org/10.5194/acp-22-13269-2022, 2022.

Elliott, H. E., Popendorf, K. J., Blades, E., Royer, H. M., Pollier, C. G. L., Oehlert, A. M., Kukkadapu, R., Ault, A., and Gaston, C. J.: Godzilla mineral dust and La Soufrière volcanic ash fallout immediately stimulate marine microbial phosphate uptake, Front. Mar. Sci., 10, https://doi.org/10.3389/fmars.2023.1308689, 2024.

Eloranta, E. W., Razenkov, I. A., Hedrick, J., and Garcia, J. P.: The design and construction of an airborne high spectral resolution lidar, in: IEEE Aerospace Conference Proceedings, https://doi.org/10.1109/AERO.2008.4526390, 2008.

Formenti, P., Schütz, L., Balkanski, Y., Desboeufs, K., Ebert, M., Kandler, K., Petzold, A., Scheuvens, D., Weinbruch, S., and Zhang, D.: Recent progress in understanding physical and chemical properties of African and Asian mineral dust, Atmos. Chem. Phys., 11, 8231–8256, https://doi.org/10.5194/acp-11-8231-2011, 2011.

Freudenthaler, V., Esselborn, M., Wiegner, M., Heese, B., Tesche, M., Ansmann, A., Müller, D., Althausen, D., Wirth, M., Fix, A., Ehret, G., Knippertz, P., Toledano, C., Gasteiger, J., Garhammer, M., and Seefeldner, M.: Depolarization ratio profiling at several wavelengths in pure Saharan dust during SAMUM 2006, Tellus B Chem. Phys. Meteorol., 61, 165, https://doi.org/10.1111/j.1600-0889.2008.00396.x, 2009.

Gasteiger, J., Groß, S., Sauer, D., Haarig, M., Ansmann, A., and Weinzierl, B.: Particle settling and vertical mixing in the Saharan Air Layer as seen from an integrated model, lidar, and in situ perspective, Atmos. Chem. Phys., 17, 297–311, https://doi.org/10.5194/acp-17-297-2017, 2017.

Gaston, C. J., Prospero, J. M., Foley, K., Pye, H. O. T., Custals, L., Blades, E., Sealy, P., and Christie, J. A.: Diverging trends in aerosol sulfate and nitrate measured in the remote North Atlantic in Barbados are attributed to clean air policies, African smoke, and anthropogenic emissions, Atmos. Chem. Phys., 24, 8049–8066, https://doi.org/10.5194/acp-24-8049-2024, 2024.

https://doi.org/10.5194/egusphere-2025-4584
Preprint. Discussion started: 25 September 2025

Giles, D. M., Sinyuk, A., Sorokin, M. G., Schafer, J. S., Smirnov, A., Slutsker, I., Eck, T. F., Holben, B. N., Lewis, J. R., Campbell, J. R., Welton, E. J., Korkin, S. V., and Lyapustin, A. I.: Advancements in the Aerosol Robotic Network (AERONET) Version 3 database – automated near-real-time quality control algorithm with improved cloud screening for Sun photometer aerosol optical depth (AOD) measurements, Atmos. Meas. Tech., 12, 169–209, https://doi.org/10.5194/amt-12-169-2019, 2019.

Groß, S., Freudenthaler, V., Schepanski, K., Toledano, C., Schäfler, A., Ansmann, A., and Weinzierl, B.: Optical properties of long-range transported Saharan dust over Barbados as measured by dual-wavelength depolarization Raman lidar measurements, Atmos. Chem. Phys., 15, 11067–11080, https://doi.org/10.5194/acp-15-11067-2015, 2015.

Groß, S., Gasteiger, J., Freudenthaler, V., Müller, T., Sauer, D., Toledano, C., and Ansmann, A.: Saharan dust contribution to the Caribbean summertime boundary layer – a lidar study during SALTRACE, Atmos. Chem. Phys., 16, 11535–11546, https://doi.org/10.5194/acp-16-11535-2016, 2016.

Guo, L., Gu, W., Peng, C., Wang, W., Li, Y. J., Zong, T., Tang, Y., Wu, Z., Lin, Q., Ge, M., Zhang, G., Hu, M., Bi, X., Wang, X., and Tang, M.: A comprehensive study of hygroscopic properties of calcium- and magnesium-containing salts: implication for hygroscopicity of mineral dust and sea salt aerosols, Atmos. Chem. Phys., 19, 2115–2133, https://doi.org/10.5194/acp-19-2115-2019, 2019.

Haarig, M., Ansmann, A., Althausen, D., Klepel, A., Groß, S., Freudenthaler, V., Toledano, C., Mamouri, R.-E., Farrell, D. A., Prescod, D. A., Marinou, E., Burton, S. P., Gasteiger, J., Engelmann, R., and Baars, H.: Triple-wavelength depolarization-ratio profiling of Saharan dust over Barbados during SALTRACE in 2013 and 2014, Atmos. Chem. Phys., 17, 10767–10794, https://doi.org/10.5194/acp-17-10767-2017, 2017.

Hayman, M. and Spuler, S.: Demonstration of a diode-laser-based high spectral resolution lidar (HSRL) for quantitative profiling of clouds and aerosols, Opt. Express, 25, A1096, https://doi.org/10.1364/OE.25.0A1096, 2017.

Holben, B. N., Eck, T. F., Slutsker, I., Tanré, D., Buis, J. P., Setzer, A., Vermote, E., Reagan, J. A., Kaufman, Y. J., Nakajima, T., Lavenu, F., Jankowiak, I., and Smirnov, A.: AERONET—A Federated Instrument Network and Data Archive for Aerosol Characterization, Remote Sens. Environ., 66, 1–16, https://doi.org/10.1016/S0034-4257(98)00031-5, 1998.

Huang, X., Yang, P., Kattawar, G., and Liou, K.-N.: Effect of mineral dust aerosol aspect ratio on polarized reflectance, J. Quant. Spectrosc. Radiat. Transf., 151, 97–109, https://doi.org/10.1016/j.jqsrt.2014.09.014, 2015.

Huang, Y., Kok, J. F., Kandler, K., Lindqvist, H., Nousiainen, T., Sakai, T., Adebiyi, A., and Jokinen, O.: Climate Models and Remote Sensing Retrievals Neglect Substantial Desert Dust Asphericity, Geophys. Res. Lett., 47, https://doi.org/10.1029/2019GL086592, 2020.

Ji, D., Palm, M., Buschmann, M., Ebell, K., Maturilli, M., Sun, X., and Notholt, J.: Hygroscopic aerosols amplify longwave downward radiation in the Arctic, Atmos. Chem. Phys., 25, 3889–3904, https://doi.org/10.5194/acp-25-3889-2025, 2025.

Kalashnikova, O. V., Garay, M. J., Martonchik, J. V., and Diner, D. J.: MISR Dark Water aerosol retrievals: operational algorithm sensitivity to particle non-sphericity, Atmos. Meas.

https://doi.org/10.5194/egusphere-2025-4584
Preprint. Discussion started: 25 September 2025

Tech., 6, 2131–2154, https://doi.org/10.5194/amt-6-2131-2013, 2013.

Kandler, K., Schneiders, K., Ebert, M., Hartmann, M., Weinbruch, S., Prass, M., and Pöhlker, C.: Composition and mixing state of atmospheric aerosols determined by electron microscopy: method development and application to aged Saharan dust deposition in the Caribbean boundary layer, Atmos. Chem. Phys., 18, 13429–13455, https://doi.org/10.5194/acp-18-13429-2018, 2018.

Karyampudi, V. M. and Carlson, T. N.: Analysis and Numerical Simulations of the Saharan Air Layer and Its Effect on Easterly Wave Disturbances, J. Atmos. Sci., 45, 3102–3136, https://doi.org/10.1175/1520-0469(1988)045<3102:AANSOT>2.0.CO;2, 1988.

Karyampudi, V. M., Palm, S. P., Reagen, J. A., Fang, H., Grant, W. B., Hoff, R. M., Moulin, C., Pierce, H. F., Torres, O., Browell, E. V., and Melfi, S. H.: Validation of the Saharan Dust Plume Conceptual Model Using Lidar, Meteosat, and ECMWF Data, Bull. Am. Meteorol. Soc., 80, 1045–1075, https://doi.org/10.1175/1520-0477(1999)080<1045:VOTSDP>2.0.CO;2, 1999.

Koehler, K. A., Kreidenweis, S. M., DeMott, P. J., Prenni, A. J., and Petters, M. D.: Potential impact of Owens (dry) Lake dust on warm and cold cloud formation, J. Geophys. Res. Atmos., 112, https://doi.org/10.1029/2007JD008413, 2007.

Kong, S., Sato, K., and Bi, L.: Lidar Ratio–Depolarization Ratio Relations of Atmospheric Dust Aerosols: The Super-Spheroid Model and High Spectral Resolution Lidar Observations, J. Geophys. Res. Atmos., 127, https://doi.org/10.1029/2021JD035629, 2022.

Li-Jones, X., Maring, H. B., and Prospero, J. M.: Effect of relative humidity on light scattering by mineral dust aerosol as measured in the marine boundary layer over the tropical Atlantic Ocean, J. Geophys. Res. Atmos., 103, 31113–31121, https://doi.org/10.1029/98JD01800, 1998.

Li, C., Li, J., Dubovik, O., Zeng, Z.-C., and Yung, Y. L.: Impact of Aerosol Vertical Distribution on Aerosol Optical Depth Retrieval from Passive Satellite Sensors, Remote Sens., 12, 1524, https://doi.org/10.3390/rs12091524, 2020.

Mahowald, N. M., Baker, A. R., Bergametti, G., Brooks, N., Duce, R. A., Jickells, T. D., Kubilay, N., Prospero, J. M., and Tegen, I.: Atmospheric global dust cycle and iron inputs to the ocean, Global Biogeochem. Cycles, 19, https://doi.org/10.1029/2004GB002402, 2005.

Marinou, E., Amiridis, V., Binietoglou, I., Tsikerdekis, A., Solomos, S., Proestakis, E., Konsta, D., Papagiannopoulos, N., Tsekeri, A., Vlastou, G., Zanis, P., Balis, D., Wandinger, U., and Ansmann, A.: Three-dimensional evolution of Saharan dust transport towards Europe based on a 9-year EARLINET-optimized CALIPSO dataset, Atmos. Chem. Phys., 17, 5893–5919, https://doi.org/10.5194/acp-17-5893-2017, 2017.

Matsuki, A., Schwarzenboeck, A., Venzac, H., Laj, P., Crumeyrolle, S., and Gomes, L.: Cloud processing of mineral dust: direct comparison of cloud residual and clear sky particles during AMMA aircraft campaign in summer 2006, Atmos. Chem. Phys., 10, 1057–1069, https://doi.org/10.5194/acp-10-1057-2010, 2010.

Mayol-Bracero, O. L., Prospero, J. M., Sarangi, B., Andrews, E., Colarco, P. R., Cuevas, E., Di Girolamo, L., Garcia, R. D., Gaston, C., Holben, B., Ladino, L. A., León, P., Losno, R., Martínez, O., Martínez-Huertas, B. L., Méndez-Lázaro, P., Molinie, J., Muller-Karger, F., Otis, D., Raga, G., Reyes, A., Rosas Nava, J., Rosas, D., Sealy, A., Serikov, I., Tong, D., Torres-Delgado, E., Yu, H., and Zuidema, P.: "Godzilla," the Extreme African Dust Event of June 2020: Origins, Transport, and Impact on Air Quality in the Greater Caribbean Basin, Bull. Am.

https://doi.org/10.5194/egusphere-2025-4584
Preprint. Discussion started: 25 September 2025

Meteorol. Soc., 106, E1620–E1648, https://doi.org/10.1175/BAMS-D-24-0045.1, 2025.

Mehra, M., Shrestha, S., AP, K., Guagenti, M., Moffett, C. E., VerPloeg, S. G., Coogan, M. A., Rai, M., Kumar, R., Andrews, E., Sherman, J. P., Flynn III, J. H., Usenko, S., and Sheesley, R. J.: Atmospheric heating in the US from saharan dust: Tracking the June 2020 event with surface and satellite observations, Atmos. Environ., 310, 119988, https://doi.org/10.1016/j.atmosenv.2023.119988, 2023.

Meloni, D., di Sarra, A., Brogniez, G., Denjean, C., De Silvestri, L., Di Iorio, T., Formenti, P., Gómez-Amo, J. L., Gröbner, J., Kouremeti, N., Liuzzi, G., Mallet, M., Pace, G., and Sferlazzo, D. M.: Determining the infrared radiative effects of Saharan dust: a radiative transfer modelling study based on vertically resolved measurements at Lampedusa, Atmos. Chem. Phys., 18, 4377–4401, https://doi.org/10.5194/acp-18-4377-2018, 2018.

Moustaka, A., Kazadzis, S., Proestakis, E., Lopatin, A., Dubovik, O., Tourpali, K., Zerefos, C., Amiridis, V., and Gkikas, A.: Enhancing dust aerosols monitoring capabilities across North Africa and the Middle East using the A-Train satellite constellation, https://doi.org/10.5194/egusphere-2025-888, 24 March 2025.

Müller, D., Weinzierl, B., Petzold, A., Kandler, K., Ansmann, A., Müller, T., Tesche, M., Freudenthaler, V., Esselborn, M., Heese, B., Althausen, D., Schladitz, A., Otto, S., and Knippertz, P.: Mineral dust observed with AERONET Sun photometer, Raman lidar, and in situ instruments during SAMUM 2006: Shape-independent particle properties, J. Geophys. Res. Atmos., 115, https://doi.org/10.1029/2009JD012520, 2010.

Müller, D., Lee, K. -H., Gasteiger, J., Tesche, M., Weinzierl, B., Kandler, K., Müller, T., Toledano, C., Otto, S., Althausen, D., and Ansmann, A.: Comparison of optical and microphysical properties of pure Saharan mineral dust observed with AERONET Sun photometer, Raman lidar, and in situ instruments during SAMUM 2006, J. Geophys. Res. Atmos., 117, https://doi.org/10.1029/2011JD016825, 2012.

O'Neill, N. T., Eck, T. F., Smirnov, A., Holben, B. N., and Thulasiraman, S.: Spectral discrimination of coarse and fine mode optical depth, J. Geophys. Res. Atmos., 108, https://doi.org/10.1029/2002JD002975, 2003.

Orozco, D., Beyersdorf, A. J., Ziemba, L. D., Berkoff, T., Zhang, Q., Delgado, R., Hennigan, C. J., Thornhill, K. L., Young, D. E., Parworth, C., Kim, H., and Hoff, R. M.: Hygrosopicity measurements of aerosol particles in the San Joaquin Valley, CA, Baltimore, MD, and Golden, CO, J. Geophys. Res. Atmos., 121, 7344–7359, https://doi.org/10.1002/2015JD023971, 2016.

Proestakis, E., Amiridis, V., Marinou, E., Georgoulias, A. K., Solomos, S., Kazadzis, S., Chimot, J., Che, H., Alexandri, G., Binietoglou, I., Daskalopoulou, V., Kourtidis, K. A., de Leeuw, G., and van der A, R. J.: Nine-year spatial and temporal evolution of desert dust aerosols over South and East Asia as revealed by CALIOP, Atmos. Chem. Phys., 18, 1337–1362, https://doi.org/10.5194/acp-18-1337-2018, 2018.

Prospero, J. M.: Mineral and sea salt aerosol concentrations in various ocean regions, J. Geophys. Res. Ocean., 84, 725–731, https://doi.org/10.1029/JC084iC02p00725, 1979.

Prospero, J. M., Delany, A. C., Delany, A. C., and Carlson, T. N.: The Discovery of African Dust Transport to the Western Hemisphere and the Saharan Air Layer: A History, Bull. Am. Meteorol. Soc., 102, E1239–E1260, https://doi.org/10.1175/BAMS-D-19-0309.1, 2021.

https://doi.org/10.5194/egusphere-2025-4584
Preprint. Discussion started: 25 September 2025

Razenkov, I.: Characterization of a Geiger-Mode Avalanche Photodiode Detector for High Special Resolution Lidar, University of Wisconsin - Madison, 2010.

Reid, E. A., Reid, J. S., Meier, M. M., Dunlap, M. R., Cliff, S. S., Broumas, A., Perry, K., and Maring, H.: Characterization of African dust transported to Puerto Rico by individual particle and size segregated bulk analysis, J. Geophys. Res. Atmos., 108, https://doi.org/10.1029/2002JD002935, 2003a.

Reid, J. S., Jonsson, H. H., Maring, H. B., Smirnov, A., Savoie, D. L., Cliff, S. S., Reid, E. A., Livingston, J. M., Meier, M. M., Dubovik, O., and Tsay, S.: Comparison of size and morphological measurements of coarse mode dust particles from Africa, J. Geophys. Res. Atmos., 108, https://doi.org/10.1029/2002JD002485, 2003b.

Riemer, N., Ault, A. P., West, M., Craig, R. L., and Curtis, J. H.: Aerosol Mixing State: Measurements, Modeling, and Impacts, Rev. Geophys., 57, 187–249, https://doi.org/10.1029/2018RG000615, 2019.

Royer, H. M., Pöhlker, M. L., Krüger, O., Blades, E., Sealy, P., Lata, N. N., Cheng, Z., China, S., Ault, A. P., Quinn, P. K., Zuidema, P., Pöhlker, C., Pöschl, U., Andreae, M., and Gaston, C. J.: African smoke particles act as cloud condensation nuclei in the wintertime tropical North Atlantic boundary layer over Barbados, Atmos. Chem. Phys., 23, 981–998, https://doi.org/10.5194/acp-23-981-2023, 2023.

Royer, H. M., Sheridan, M. T., Elliott, H. E., Lata, N. N., Cheng, Z., China, S., Zhu, Z., Ault, A. P., and Gaston, C. J.: African dust transported to Barbados in the Wintertime Lacks Indicators of Chemical Aging, Atmos. Chem. Phys., https://doi.org/10.5194/egusphere-2024-3288, 2025.

Russell, P. B., Bergstrom, R. W., Shinozuka, Y., Clarke, A. D., DeCarlo, P. F., Jimenez, J. L., Livingston, J. M., Redemann, J., Dubovik, O., and Strawa, A.: Absorption Angstrom Exponent in AERONET and related data as an indicator of aerosol composition, Atmos. Chem. Phys., 10, 1155–1169, https://doi.org/10.5194/acp-10-1155-2010, 2010.

Scheuvens, D., Schütz, L., Kandler, K., Ebert, M., and Weinbruch, S.: Bulk composition of northern African dust and its source sediments — A compilation, Earth-Science Rev., 116, 170–194, https://doi.org/10.1016/j.earscirev.2012.08.005, 2013.

Shao, L., Liu, P., Jones, T., Yang, S., Wang, W., Zhang, D., Li, Y., Yang, C.-X., Xing, J., Hou, C., Zhang, M., Feng, X., Li, W., and BéruBé, K.: A review of atmospheric individual particle analyses: Methodologies and applications in environmental research, Gondwana Res., 110, 347–369, https://doi.org/10.1016/j.gr.2022.01.007, 2022.

Shen, H., Peters, T. M., Casuccio, G. S., Lersch, T. L., West, R. R., Kumar, A., Kumar, N., and Ault, A. P.: Elevated Concentrations of Lead in Particulate Matter on the Neighborhood-Scale in Delhi, India As Determined by Single Particle Analysis, Environ. Sci. Technol., 50, 4961–4970, https://doi.org/10.1021/acs.est.5b06202, 2016.

Tesche, M., Müller, D., Gross, S., Ansmann, A., Althausen, D., Freudenthaler, V., Weinzierl, B., Veira, A., and Petzold, A.: Optical and microphysical properties of smoke over Cape Verde inferred from multiwavelength lidar measurements, Tellus B Chem. Phys. Meteorol., 63, 677, https://doi.org/10.1111/j.1600-0889.2011.00549.x, 2011.

Titos, G., Cazorla, A., Zieger, P., Andrews, E., Lyamani, H., Granados-Muñoz, M. J., Olmo, F. J., and Alados-Arboledas, L.: Effect of hygroscopic growth on the aerosol light-scattering

https://doi.org/10.5194/egusphere-2025-4584
Preprint. Discussion started: 25 September 2025

coefficient: A review of measurements, techniques and error sources, Atmos. Environ., 141, 494–507, https://doi.org/10.1016/j.atmosenv.2016.07.021, 2016.

Tsamalis, C., Chédin, A., Pelon, J., and Capelle, V.: The seasonal vertical distribution of the Saharan Air Layer and its modulation by the wind, Atmos. Chem. Phys., 13, 11235–11257, https://doi.org/10.5194/acp-13-11235-2013, 2013.

Weinzierl, B., Ansmann, A., Prospero, J. M., Althausen, D., Benker, N., Chouza, F., Dollner, M., Farrell, D., Fomba, W. K., Freudenthaler, V., Gasteiger, J., Groß, S., Haarig, M., Heinold, B., Kandler, K., Kristensen, T. B., Mayol-Bracero, O. L., Müller, T., Reitebuch, O., Sauer, D., Schäfler, A., Schepanski, K., Spanu, A., Tegen, I., Toledano, C., and Walser, A.: The Saharan Aerosol Long-Range Transport and Aerosol–Cloud-Interaction Experiment: Overview and Selected Highlights, Bull. Am. Meteorol. Soc., 98, 1427–1451, https://doi.org/10.1175/BAMS-D-15-00142.1, 2017.

Winkler, P.: The growth of atmospheric aerosol particles as a function of the relative humidity—II. An improved concept of mixed nuclei, J. Aerosol Sci., 4, 373–387, https://doi.org/10.1016/0021-8502(73)90027-X, 1973.

World Health Organization: WHO global air quality guidlines. Particulate matter (PM2.5 and PM10), ozone, nitrogen dioxide, sulfur dioxide and carbon monoxide, Geneva, 290 pp., 2021.

Xian, P., Reid, J. S., Hyer, E. J., Sampson, C. R., Rubin, J. I., Ades, M., Asencio, N., Basart, S., Benedetti, A., Bhattacharjee, P. S., Brooks, M. E., Colarco, P. R., da Silva, A. M., Eck, T. F., Guth, J., Jorba, O., Kouznetsov, R., Kipling, Z., Sofiev, M., Perez Garcia-Pando, C., Pradhan, Y., Tanaka, T., Wang, J., Westphal, D. L., Yumimoto, K., and Zhang, J.: Current state of the global operational aerosol multi-model ensemble: An update from the International Cooperative for Aerosol Prediction (ICAP), Q. J. R. Meteorol. Soc., 145, 176–209, https://doi.org/10.1002/qj.3497, 2019.

Yang, L., Zhang, S., Tao, H., Yang, Y., Wang, L., Cui, Y., Xu, Y., and Li, X.: Comprehensive Analysis of a Dust Storm by a Lidar Network Combined With Multiple Data, Front. Environ. Sci., 10, https://doi.org/10.3389/fenvs.2022.832710, 2022.

Yang, W., Marshak, A., Várnai, T., Kalashnikova, O. V., and Kostinski, A. B.: CALIPSO observations of transatlantic dust: vertical stratification and effect of clouds, Atmos. Chem. Phys., 12, 11339–11354, https://doi.org/10.5194/acp-12-11339-2012, 2012.

Zhang, X., Massoli, P., Quinn, P. K., Bates, T. S., and Cappa, C. D.: Hygroscopic growth of submicron and supermicron aerosols in the marine boundary layer, J. Geophys. Res. Atmos., 119, 8384–8399, https://doi.org/10.1002/2013JD021213, 2014.

Zuidema, P., Alvarez, C., Kramer, S. J., Custals, L., Izaguirre, M., Sealy, P., Prospero, J. M., and Blades, E.: Is Summer African Dust Arriving Earlier to Barbados? The Updated Long-Term In Situ Dust Mass Concentration Time Series from Ragged Point, Barbados, and Miami, Florida, Bull. Am. Meteorol. Soc., 100, 1981–1986, https://doi.org/10.1175/BAMS-D-18-0083.1, 2019.